polymers

MDPI

Article

Fatigue Behavior of Rotary Friction Welding of Acrylonitrile Butadiene Styrene and Polycarbonate Dissimilar Materials

Chil-Chyuan Kuo [1,2,3,4,*], Naruboyana Gurumurthy [1,5] and Song-Hua Hunag [6]

[1] Department of Mechanical Engineering, Ming Chi University of Technology, No. 84, Gungjuan Road, Taishan District, New Taipei City 24301, Taiwan
[2] Research Center for Intelligent Medical Devices, Ming Chi University of Technology, No. 84, Gungjuan Road, Taishan District, New Taipei City 24301, Taiwan
[3] Department of Mechanical Engineering, Chang Gung University, No. 259, Wenhua 1st Rd., Guishan Dist., Taoyuan City 33302, Taiwan
[4] Center for Reliability Engineering, Ming Chi University of Technology, No. 84, Gungjuan Road, Taishan District, New Taipei City 24301, Taiwan
[5] Department of Mechanical Engineering, Presidency University, Rajankunte, Near Yelhanka, Bangalore 700073, India
[6] Li-Yin Technology Co., Ltd., No. 37, Lane 151, Section 1, Zhongxing Road, Wugu District, New Taipei City 24101, Taiwan
* Correspondence: jacksonk@mail.mcut.edu.tw

Abstract: Understanding the fatigue behaviors of weld joints is significant in engineering practice. Rotary friction welding (RFW) can join the additively manufactured polymer components. Until now, no research has focused on the fatigue behavior of polymer components jointed via RFW. This study investigates the fatigue life of ABS/PC dissimilar components fabricated via RFW and proposes the fatigue mechanism based on the failure structure. This work uses five different cyclic loads and rotational speeds to investigate the fatigue life. The fatigue life of the RFW of ABS/PC dissimilar rods is better compared with the pure ABS and pure PC specimens due to weld and integrity microstructural changes resulting from the combination of ABS and PC materials. The number of cycles until the rupture of RFW of ABS/PC dissimilar components (y) can be determined by the cyclic load (x) according to the prediction equation of $y = -838.25x^2 - 2035.8x + 67{,}262$. The fatigue life of the RFW of ABS/PC dissimilar components increase with the increased rotational speed. The number of cycles until rupture (y) can be determined by the different rotational speeds (x) according to the prediction equation of $y = 315.21x^2 + 2710.4x + 32{,}124$.

Keywords: rotary friction welding; fatigue life; fatigue failure mechanism; number of cycles to rupture; rotational speed; cyclic load

Citation: Kuo, C.-C.; Gurumurthy, N.; Hunag, S.-H. Fatigue Behavior of Rotary Friction Welding of Acrylonitrile Butadiene Styrene and Polycarbonate Dissimilar Materials. *Polymers* **2023**, *15*, 3424. https://doi.org/10.3390/polym15163424

Academic Editors: David Alexander Gregory and Yu Zhang

Received: 16 July 2023
Revised: 9 August 2023
Accepted: 15 August 2023
Published: 16 August 2023

1. Introduction

The rotary friction welding (RFW) [1–3] of dissimilar materials is helpful in current industries, such as the automotive, aircraft, aerospace, and marine industries. RFW provides a lower energy consumption and environmental impact compared with fusion welding [4,5]. RFW needs very little heat and friction applied to the components during the welding process [6]. Therefore, this technology is frequently used to join metals or polymers [7]. Bhukya et al. [8] investigated its effect on the mechanical properties, downward force, and temperature profile of an aluminum alloy using friction stir welding. The results revealed that low force was decreased after introducing the copper donor. The surface hardness was reduced from the base metal to the center of the weld interface. Zhan et al. [9] predicted the fatigue life of the welding tool during the friction stir welding of an aluminum alloy. The results showed that the fatigue life of the welding tools was increased with the increase in the rotational speed. It was found that the compressive stress on the welding tool was at the back side and the tensile stress on the welding tool was at the front side. Shi et al. [10]

employed laser welding to join the additive manufactured parts. The results indicated that the weld joint of the Al–Cu alloy was nearly free of defects. Liu et al. [11] reviewed the fatigue behavior of clinched joints, including their life estimation model, influencing factors, fatigue strength, and failure mechanism. Rayan et al. [12] investigated the fatigue behavior of maraging steel components. The results indicated that the mechanical property of maraging steel components was decreased by the reuse of maraging steel powder. Ahmed et al. [13] investigated the fatigue properties of aluminum alloys. The results showed that the weld joint with the 1.4 wt.% Mg filler provided the best fatigue life and highest fatigue strength. Su et al. [14] studied the fatigue behavior of tube connections under cyclic pressure. The results showed that the proposed method should be frequently used in un-welded and welded structures because it is easy to operate, is reliable, and is safe. Visco et al. [15] analyzed weld joints using static mechanical tests. The results revealed that the joints had an appreciable resistance to fatigue. Yu et al. [16] investigated the fatigue behavior of weld joints strengthened with carbon-fiber-reinforced polymer laminates. It was found that the predicted fatigue life was consistent with the experimental result. Koller et al. [17] identified an adhesive system suitable for achieving a high fatigue strength in a carbon-fiber-reinforced polymer patch. The results showed that the compressive nominal stress promoted the crack closure effect. Popescu et al. [18] investigated the fatigue behavior of polylactic acid orthoses. The results showed that the minimum force was approximately 95 N, reaching 110 N after 1100–1200 cycles during fatigue tests.

In the consumer electronics industry, acrylonitrile butadiene styrene (ABS) [19] and polycarbonate (PC) [20] are extensively employed in some critical components because they are more lightweight than metal. ABS has a high tensile strength and physical impacts. ABS plastic is suitable for making consumer products that withstand heavy use. PC plastic is also an engineering thermoplastic because it has excellent heat resistance. Therefore, both PC and ABS are widely used in the consumer electronics industry. However, few studies focus on the fatigue life of ABS/PC polymer rods jointed via RFW. According to practical experience, the welded parts' reliability [21,22] is related to the fatigue life [23]. The main objective of this study was to investigate the fatigue life [24] of the polymer rods with five different cyclic loads. The fracture surfaces after the fatigue test were examined using an optical microscope (OM). Both fatigue life and fatigue behaviors were analyzed. Finally, the fatigue mechanism of the ABS/PC polymer rods was proposed.

2. Experimental Details

Figure 1 shows the flowchart of the research process used in this study. The objective was to study the fatigue behavior of the polymers. Figure 2 shows the size and geometry of the fatigue test specimen. The fatigue test specimen was also a cylindrical rod with a diameter of 15 mm and a length of 150 mm. The specimens were printed using a three-dimensional printing apparatus called fused deposition modeling (FDM) (Teklink smart solution Inc., New Taipei City, Taiwan) with two different kinds of thermoplastic filaments, i.e., ABS (Thunder 3D Inc., New Taipei City, Taiwan) and PC (Thunder 3D Inc., New Taipei City, Taiwan) [25–27]. The printing parameters for the ABS specimens involved a printing bed temperature of 100 °C, a printing speed of 80 mm/s, a printing temperature of 230 °C, and a layer thickness of 0.4 mm [28]. The printing parameters for manufacturing the PC specimens included a printing bed temperature of 100 °C, a printing speed of 80 mm/s, a printing temperature of 245 °C, and a layer thickness of 0.4 mm [29].

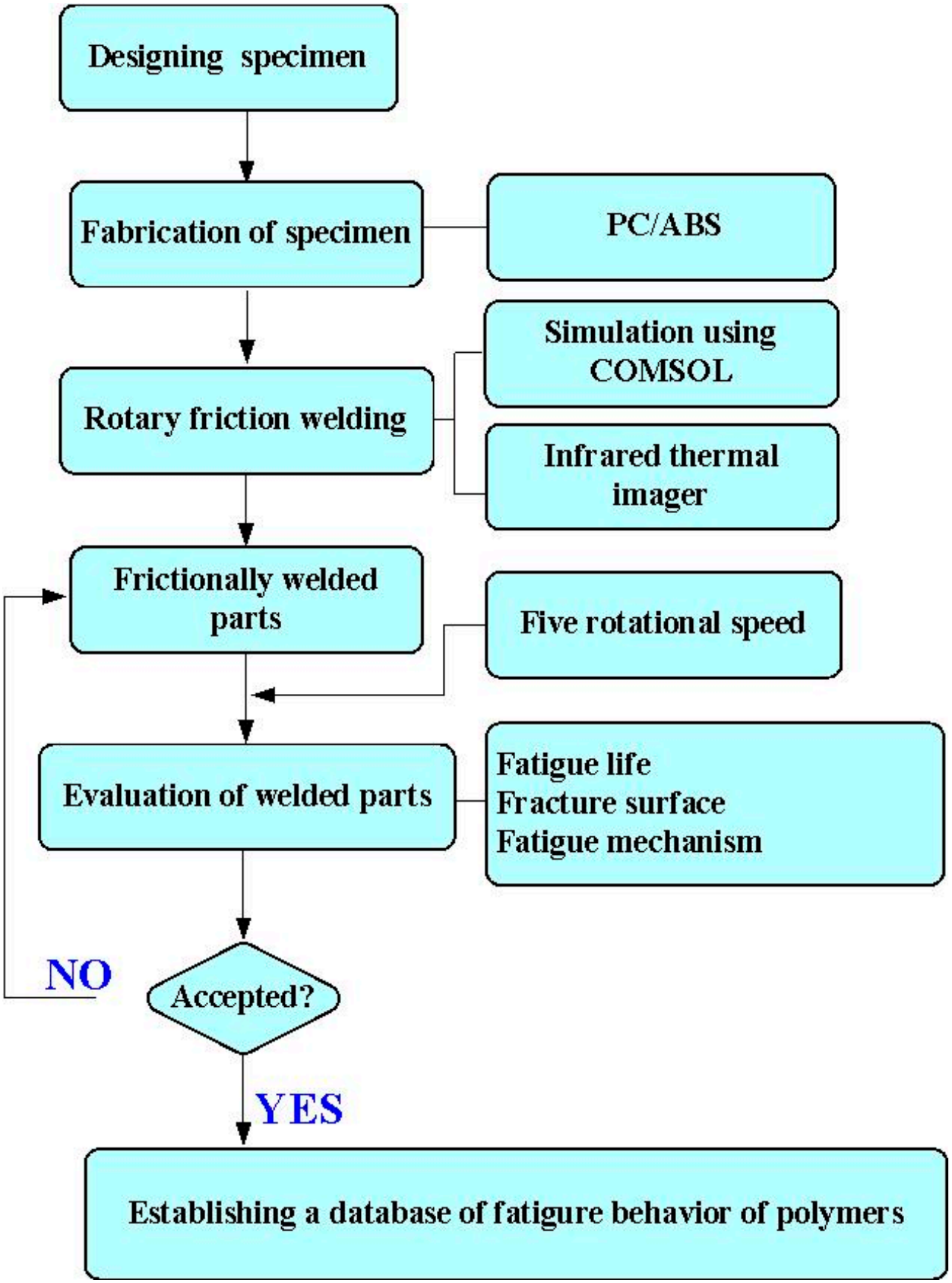

Figure 1. Flowchart of the research process used in this study.

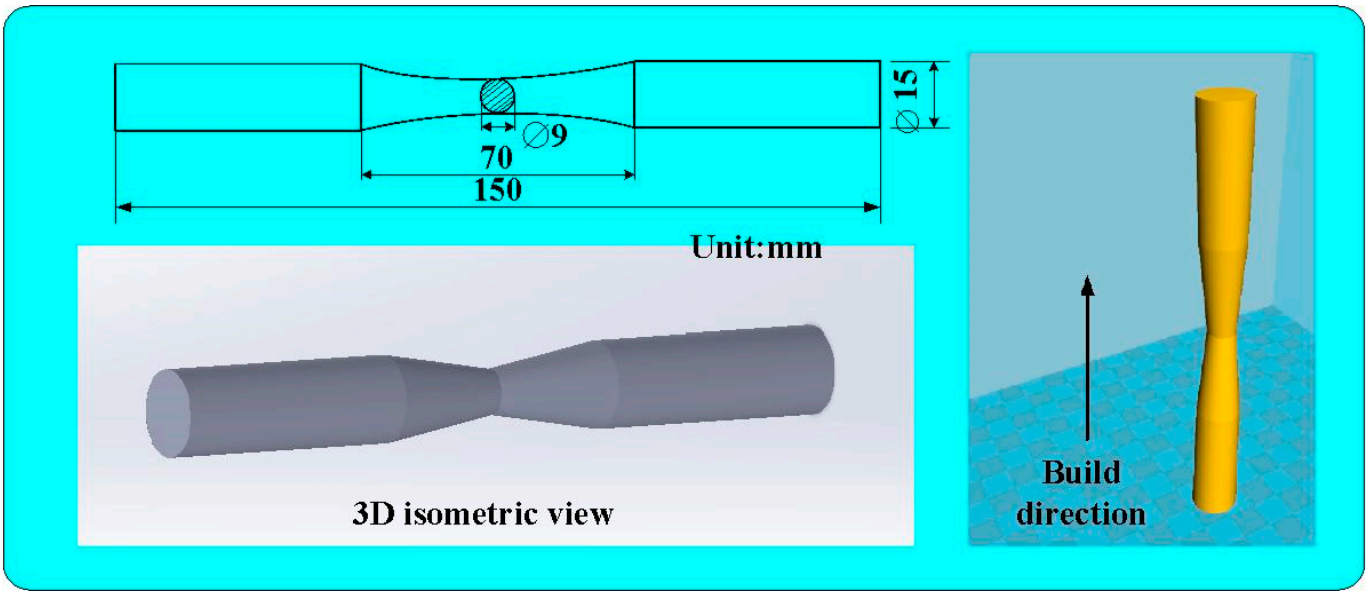

Figure 2. The size and geometry of the fatigue test specimen.

In this work, a turning machine was used for RFW. The welding parameters included an axial load of 17 N, a feed rate of 0.1 mm/min, a friction time of 20 s, a welding time of 20 s, and a burn-off length of 2 mm. To investigate the effects of the rotational speed of RFW on the fatigue life of welded parts, five different rotational speeds were assessed in this study, i.e., 330, 490, 650, 950, and 1350 rpm. During RFW, the temperature history in the weld joint was recorded using an infrared thermal imager [30] (BI-TM-F01P, Panrico trading Inc., New Taipei City, Taiwan). Significantly, the temperature history in the weld joint was also predicted using COMSOL Multiphysics software. Figure 3 shows the schematic illustration of the RFW process used to make a fatigue test sample. After RFW, the fatigue tests were performed on pure ABS, pure PC, the RFW of ABS/ABS, the RFW of PC/ABS, as well as the RFW of ABS/PC rods using a rotating-beam fatigue test (3LMF03U801, Taiwan Nakazawa Co., Ltd., Taichung, Taiwan). Figure 4 shows the experimental setup for the fatigue life of the welded parts. To investigate the effects of loads on the fatigue life of the welded parts, five different loads were assessed in this work, i.e., 1, 2, 3, 4, and 5 kg. After the fatigue tests, the fatigue fracture surfaces were investigated comprehensively using an optical microscope. A fatigue mechanism was proposed according to the fatigue fracture surfaces. After the fatigue test, the fracture surface was analyzed using a stereo OM (Quick Vision 404, Mitutoyo Inc., Tokyo, Japan) and FE-SEM (JEC3000-FC, JEOL Inc., Tokyo, Japan).

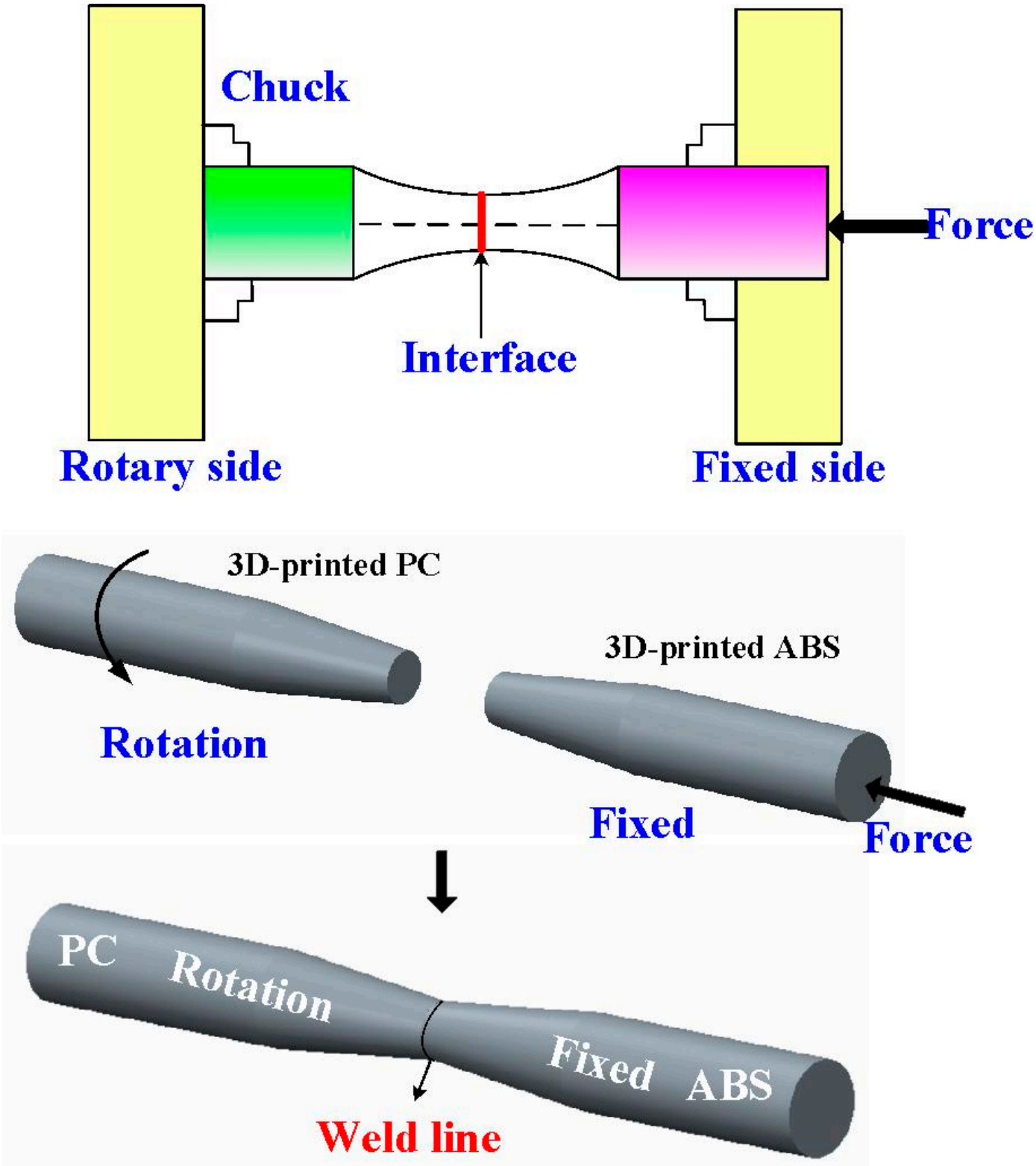

Figure 3. Schematic illustration of the RFW process used to make a fatigue test sample.

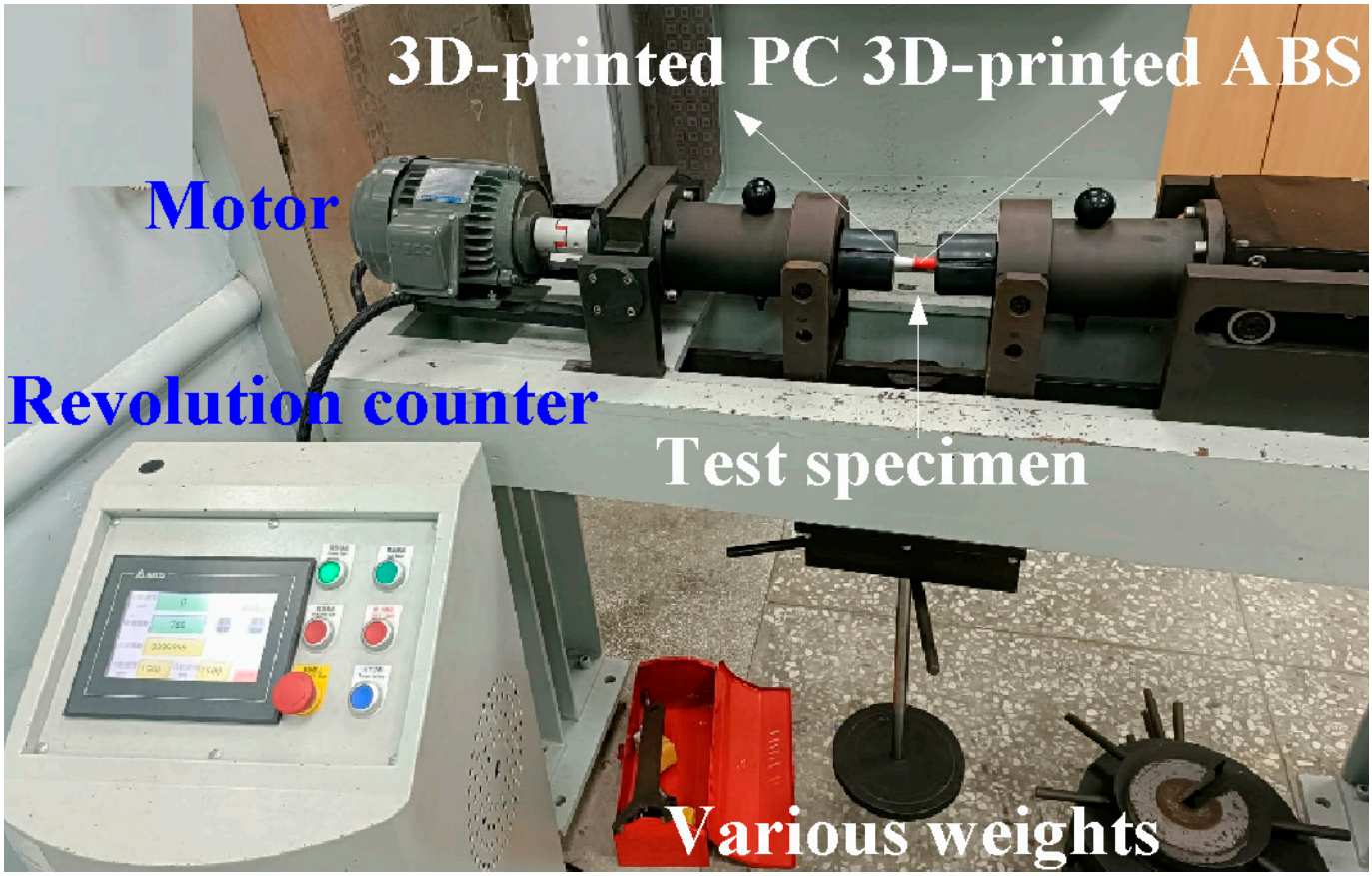

Figure 4. Experimental setup for the fatigue life of the welded parts.

3. Results and Discussion

The fatigue behavior of the RFW joints was evaluated using a rotating-beam fatigue-testing machine. In this study, three different fatigue samples were used to investigate the fatigue behavior. Two fatigue samples were 3D printed in PC and ABS using a fused deposition modeling apparatus. The other fatigue sample comprised 3D-printed PC and 3D-printed ABS joined using RFW. Figure 5 shows the test specimens for the fatigue test. After the fatigue tests, the fatigue fracture surfaces of solid ABS, solid PC, and the RFW of ABS/PC were investigated comprehensively using an optical microscope. Figure 6 shows the fatigue test results. For the welded part of the RFW of ABS/PC, the fractured location appears in the ABS polymer rod. For the welded part of the RFW of PC/PC, the fractured location appears in the weld interface. For the welded part of the RFW of ABS/ABS, the fractured location appears in the weld interface. Figure 7 shows the fatigue failure surface of pure PC. Figure 8 shows the fatigue failure surface of pure ABS. Figure 9 shows the fatigue failure surface of the RFW of ABS/PC. As can be seen, two distinct zones were found, i.e., a slow fracture zone and fast fracture zone. The original stands for the crack started during the fatigue test. In the fatigue zone, the crack grew gradually. The progression marks indicate the trend observed in the growth of the crack. In the overload zone, the crack grew quickly. Two different results were found. One is that the fatigue failure mechanism of polymers is the same as that of metals [31]. The other one is that the fatigue failure mechanism of welded parts produced via the RFW of PC and ABS dissimilar rods is the same as that of pure ABS or pure PC rods. This result shows that the welding quality of the RFW of PC and ABS dissimilar rods is robust. It should be noted that the fractured location appears in the ABS rods after the fatigue test, which is same as the bending test [32].

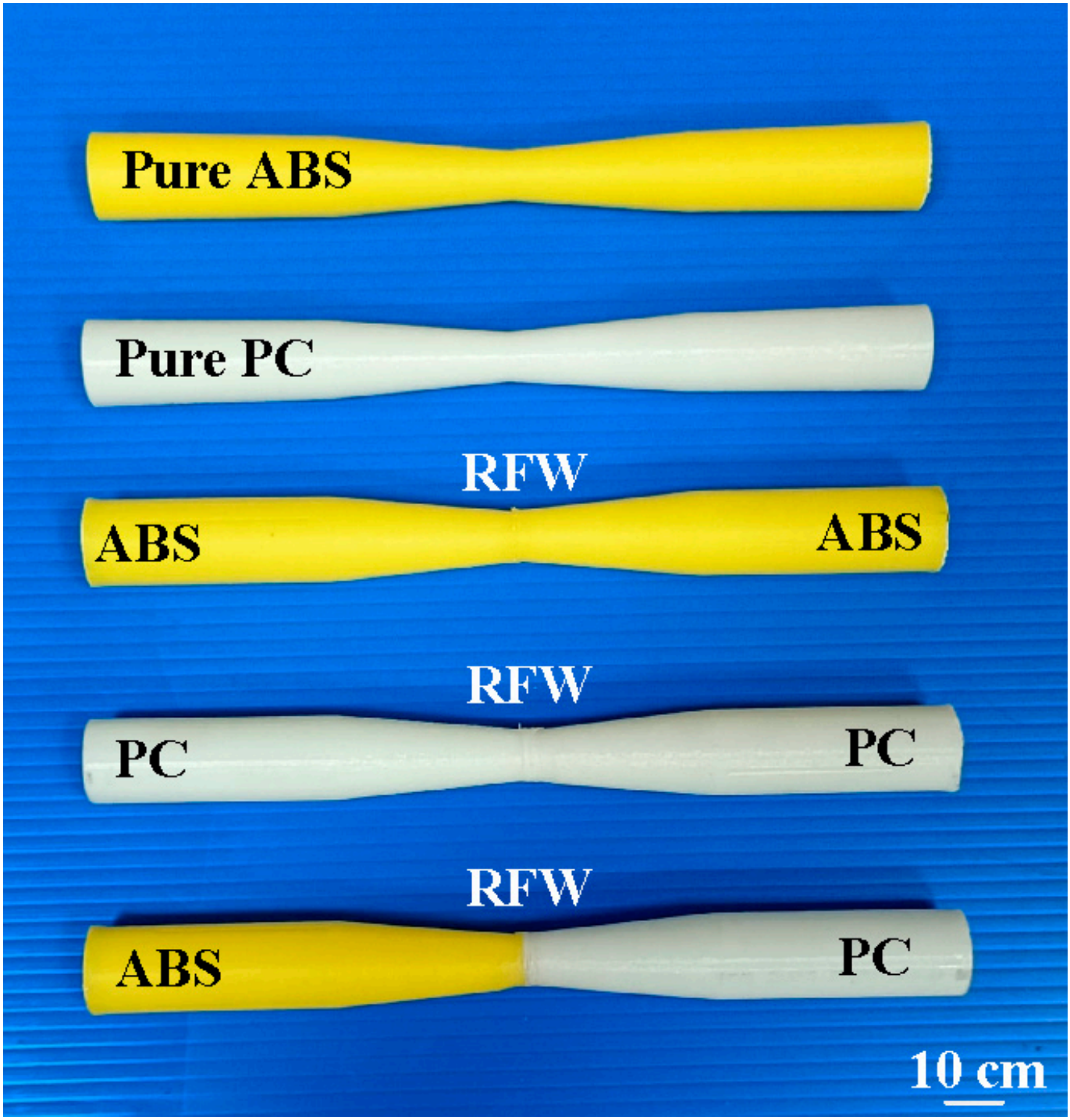

Figure 5. Test specimens for the fatigue test.

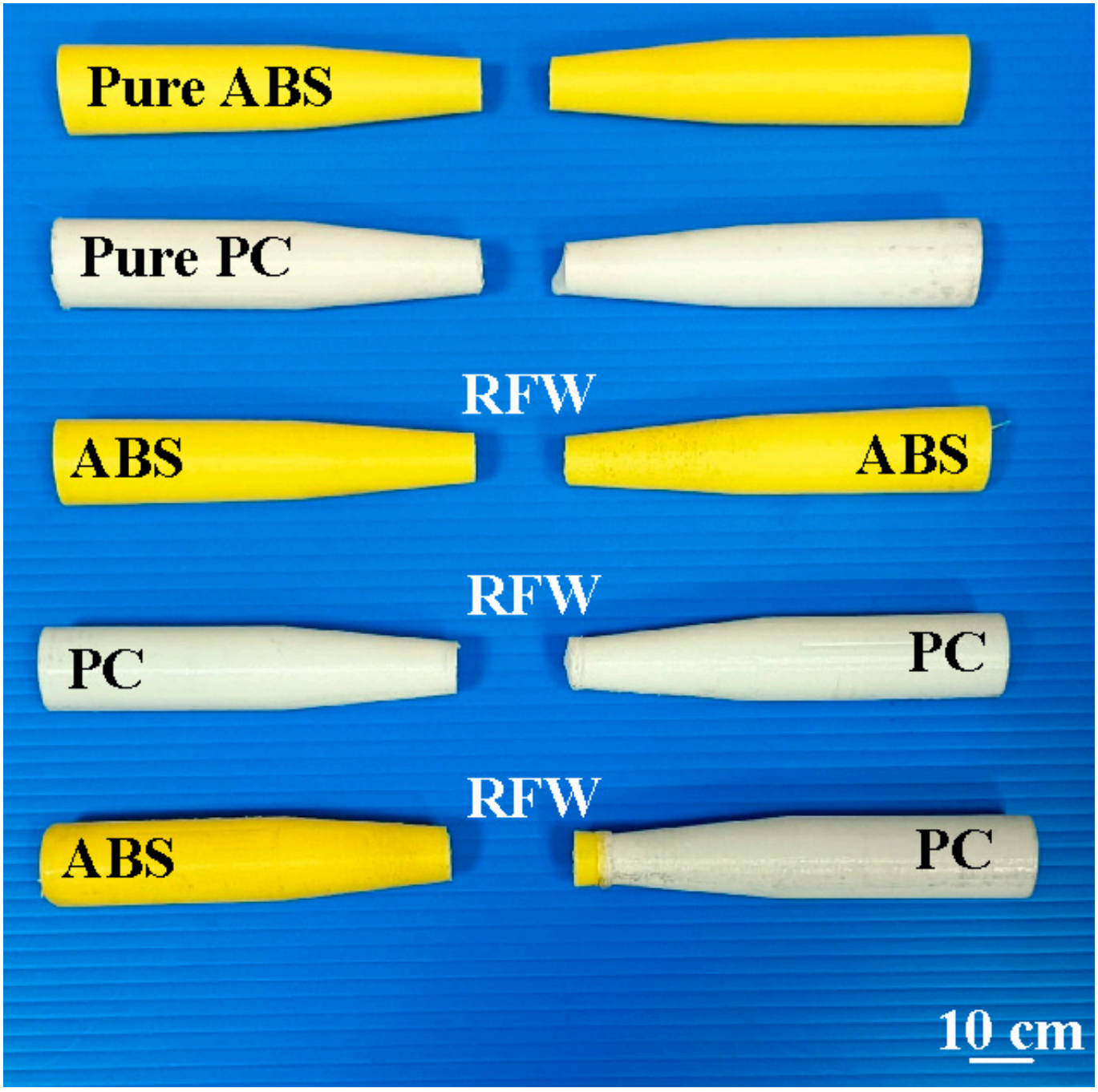

Figure 6. Fatigue test results.

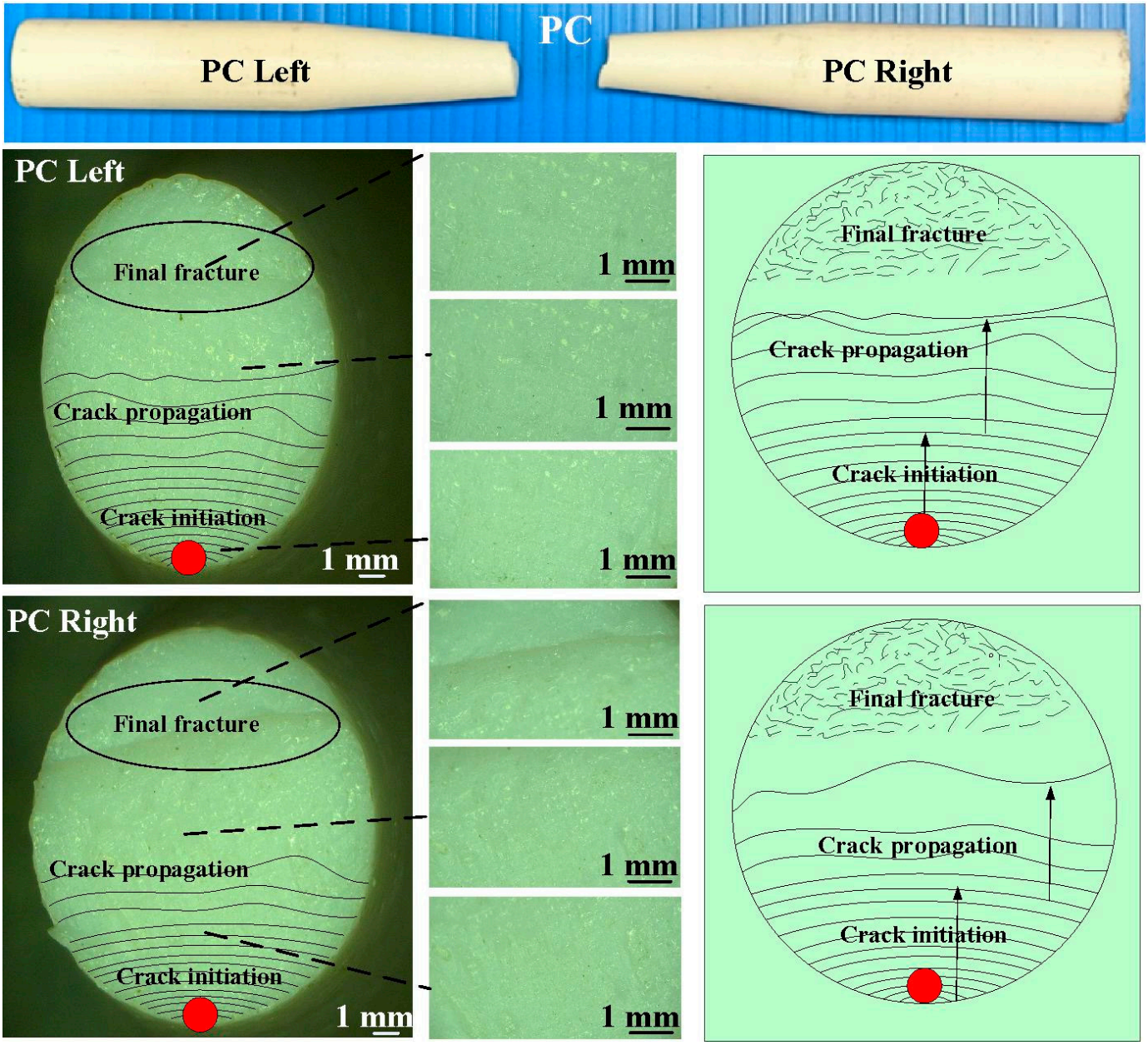

Figure 7. Fatigue failure surface of pure PC.

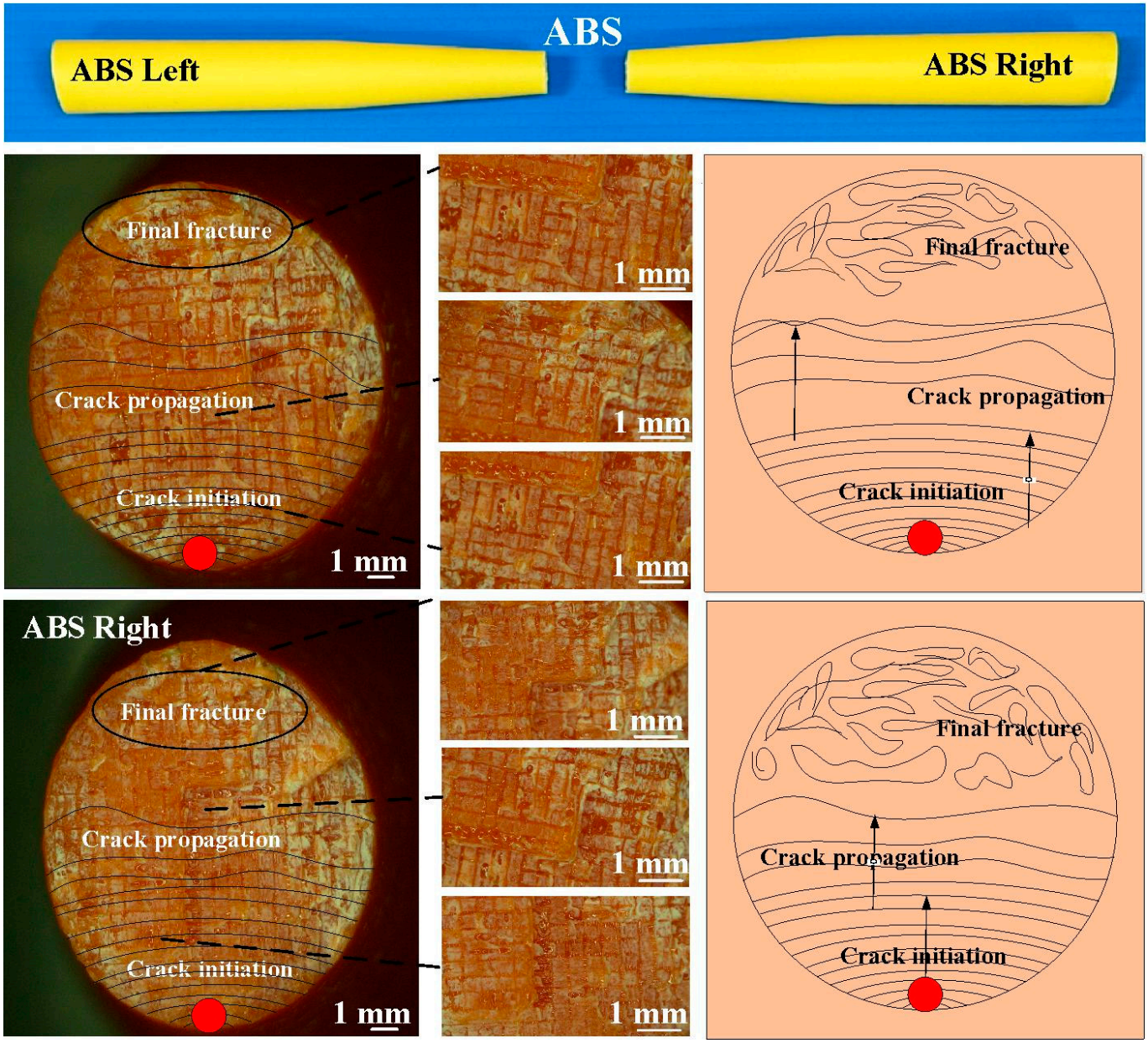

Figure 8. Fatigue failure surface of pure ABS.

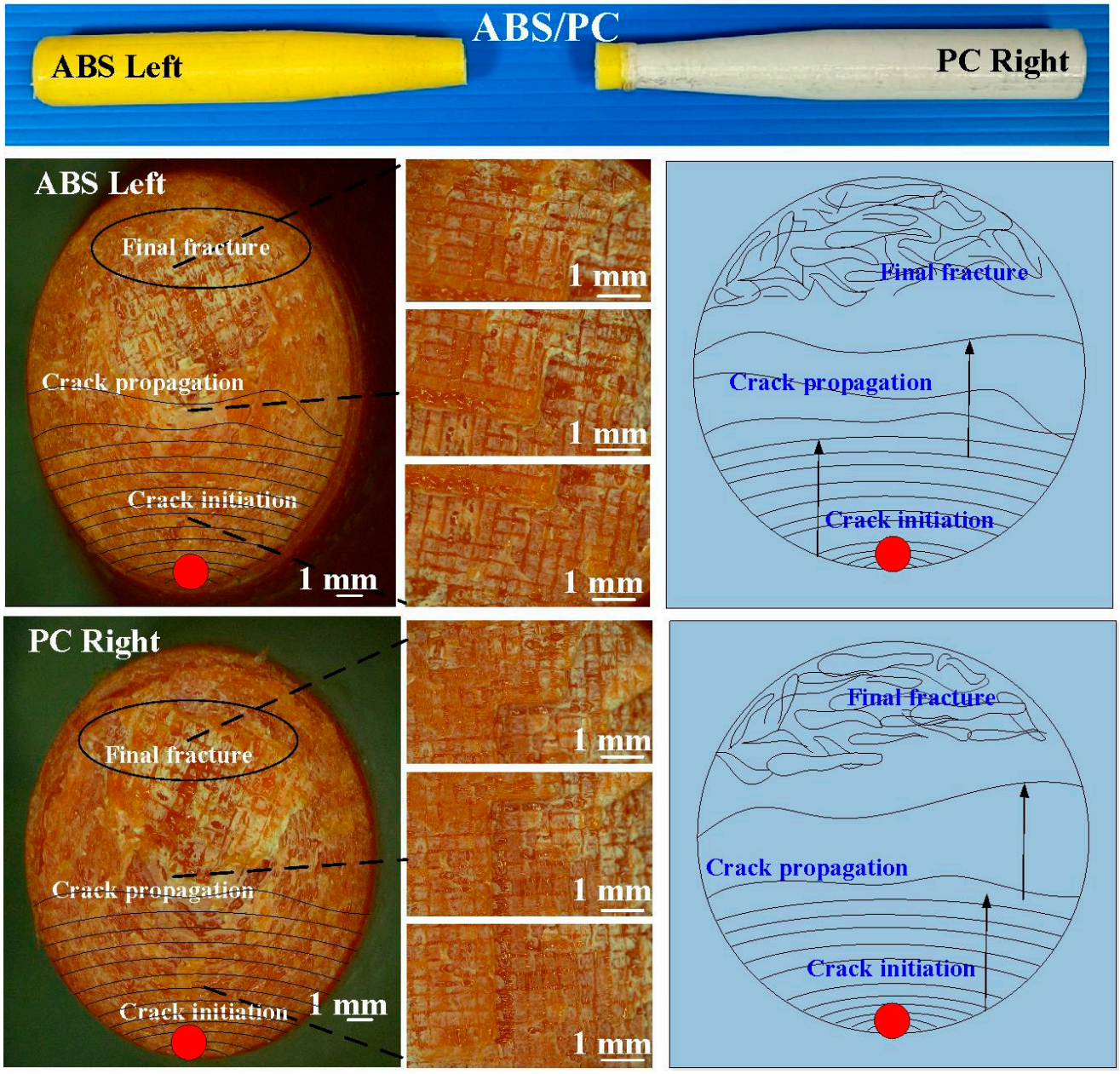

Figure 9. Fatigue failure surface of the RFW of ABS/PC.

In this study, five specimens were assessed. Figure 10 shows the fatigue test results of the pure PC rods under five different cyclic loads. The results showed that the average number of cycles until rupture was about 29,706, 20,140, 18,024, 14,796, and 13,796 when the pure PC fatigue test specimens were subjected to five different loads of 1, 2, 3, 4, and 5 kg. As can be seen, the fatigue life of the pure PC fatigue test piece was shorter under a higher load. Based on the experimental results obtained for a cyclic load of 1 kg, the reduction ratios of the cycles until rupture for four different loads of 2, 3, 4, and 5 kg were about 32.20, 39.33, 50.19, and 53.56%, respectively. It should be pointed out that the average number of cycles until rupture (y) can be determined by the cyclic load (x) according to the prediction equation of $1144.3x^2 - 10{,}582x + 38{,}452$, with a correlation coefficient (R^2) of 0.9705. Figure 11 shows the fatigue test results of the pure ABS rods under five different loads. The results showed that the average number of cycles until rupture was about 25,400, 17,370, 14,372, 10,718, and 9502 when the pure ABS fatigue test specimens were subjected to five different loads of 1, 2, 3, 4, and 5 kg.

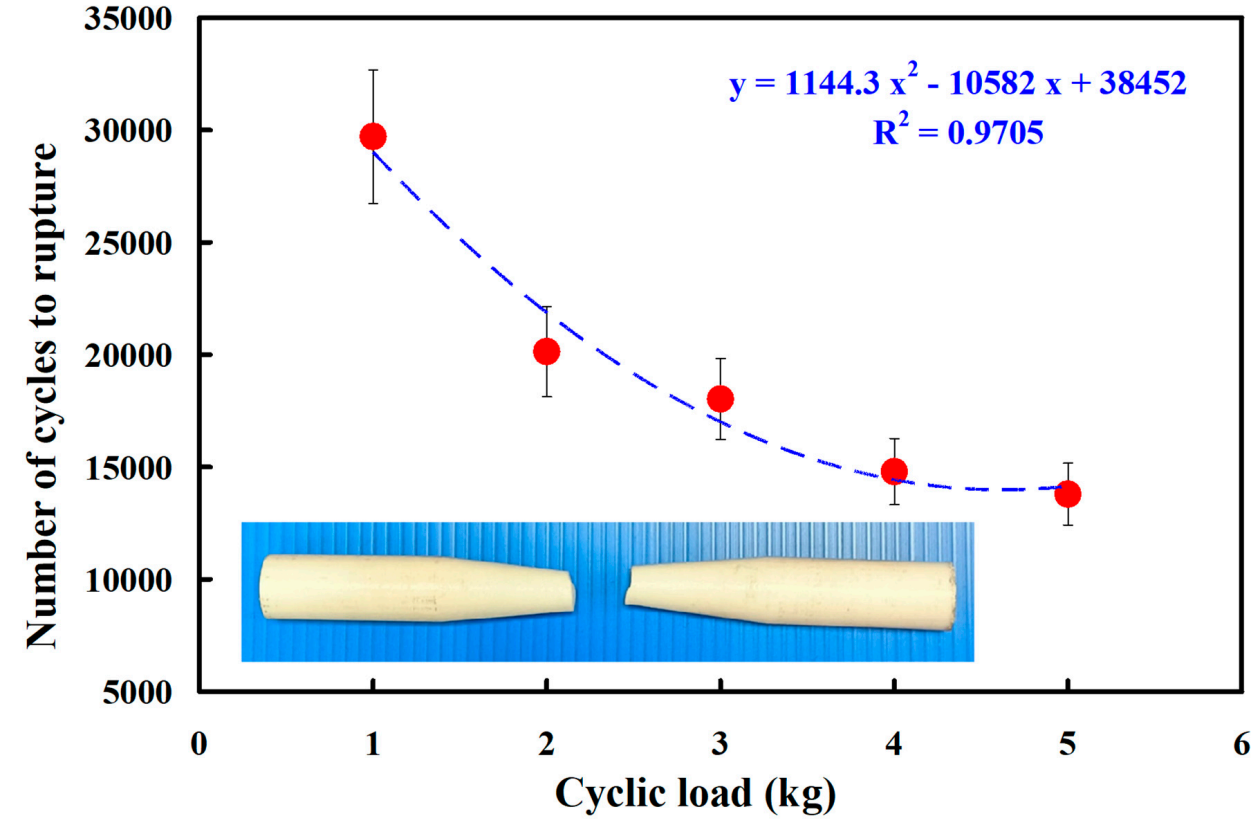

Figure 10. Fatigue test results of pure PC rods under five different cyclic loads.

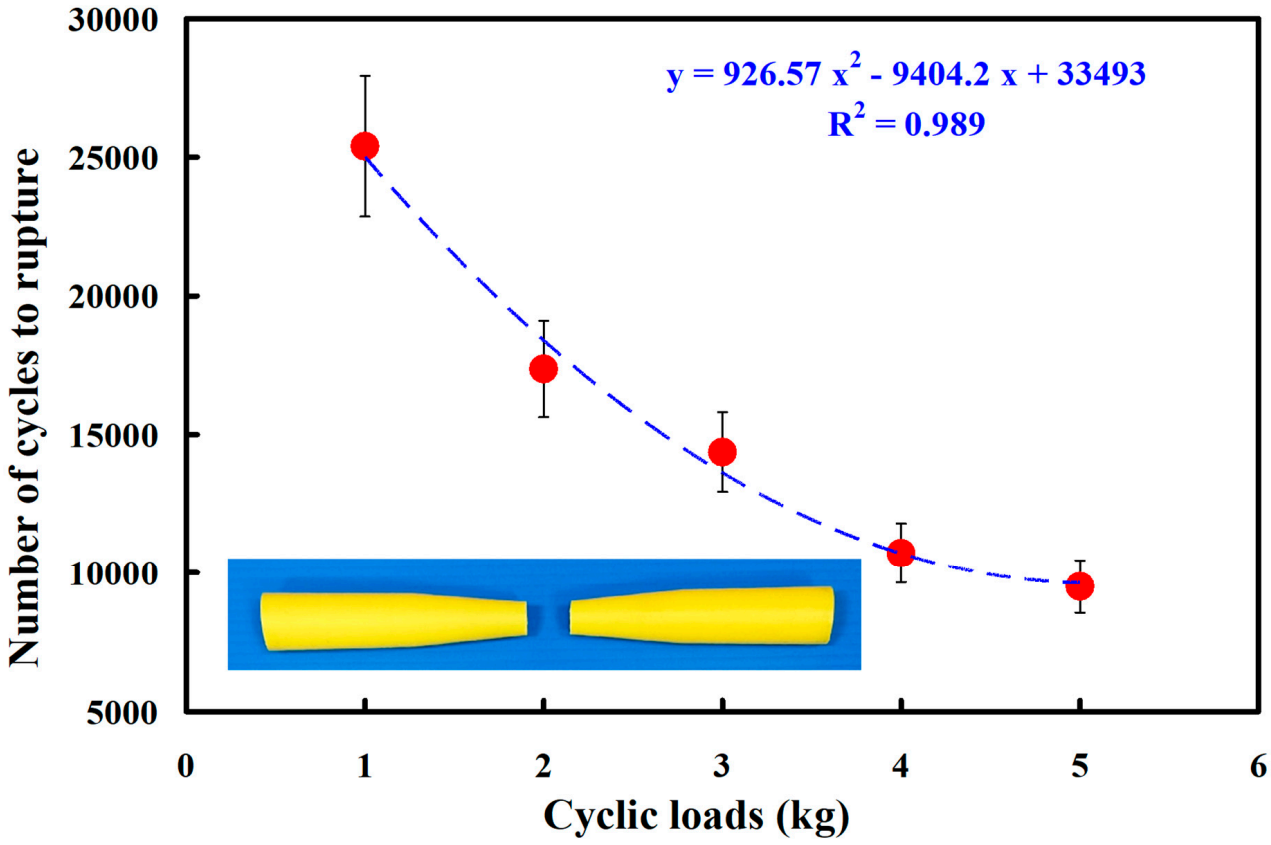

Figure 11. Fatigue test results of pure ABS rods under five different cyclic loads.

As a result, the average number of cycles until rupture (y) can be determined by the cyclic load (x) according to the prediction equation of $y = 926.57x^2 - 9404.2x + 33{,}493$, with a correlation coefficient of 0.989.

Figure 12 shows the fatigue test results of the RFW of PC and PC similar rods under five different cyclic loads. The results showed that the average number of cycles until rupture was about 76,027, 66,185, 59,234, 48,950, and 39,205 when the fatigue test specimens were subjected to five different loads of 1 kg, 2 kg, 3 kg, 4 kg, and 5 kg. As a result, the number of cycles until rupture (y) can be determined by the cyclic load (x) according to the prediction equation of $-195.98x^3 + 1539.7x^2 - 12{,}368x + 86{,}907$, with a correlation coefficient of 0.9982. Figure 13 shows the fatigue test results of the RFW of ABS and ABS similar rods under five different cyclic loads. The results showed that the average number of cycles until rupture was about 52,569, 45,059, 40,758, 30,127, and 27,634 when the fatigue test specimens were subjected to five different loads of 1 kg, 2 kg, 3 kg, 4 kg, and 5 kg. As a result, the number of cycles until rupture (y) can be determined by the cyclic load (x) according to the prediction equation of $410.63x^3 - 3431.1x^2 + 1623.3x + 53{,}623$, with a correlation coefficient of 0.9809.

Figure 14 shows the fatigue test results of the RFW of ABS/PC dissimilar rods under five different cyclic loads. The results showed that the average number of cycles until rupture was about 63,850, 60,701, 54,254, 43,988, and 36,880 when the fatigue test specimens were subjected to five different loads of 1, 2, 3, 4, and 5 kg. The number of cycles until rupture (y) can be determined by the cyclic load (x) according to the prediction equation of $-838.25x^2 - 2035.8x + 67{,}262$, with a correlation coefficient of 0.9903. Figure 15 shows the fatigue test results of the five different fatigue test specimens under five different cyclic loads. It should be noted that the fatigue life of the RFW of PC/PC dissimilar rods is the best due to the weld integrity resulting from the combination of PC and PC materials after RFW [33]. The fatigue life of the RFW of ABS/ABS similar rods is the worst. The fatigue life of the RFW of ABS/PC dissimilar rods is in between. These results are consistent with the mechanical properties of the welding base metal [34–36].

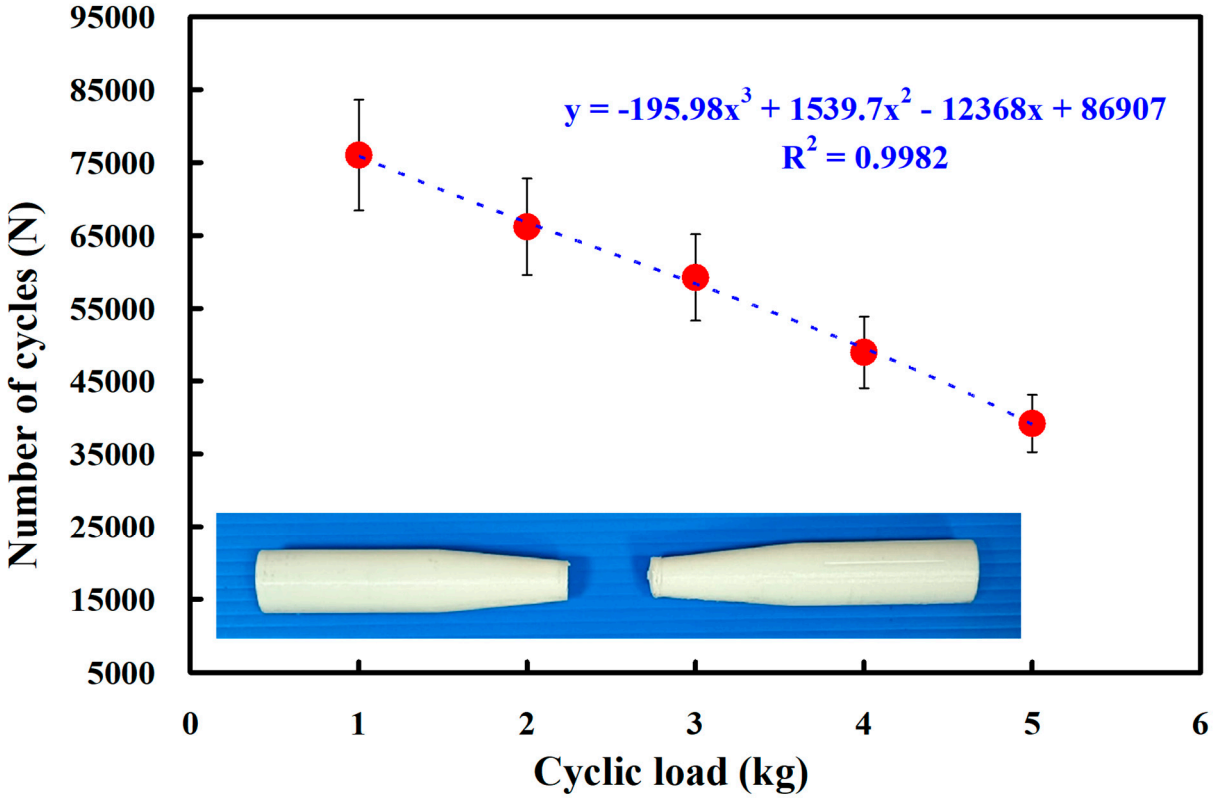

Figure 12. Fatigue test results of the RFW of PC and PC similar rods under five different cyclic loads.

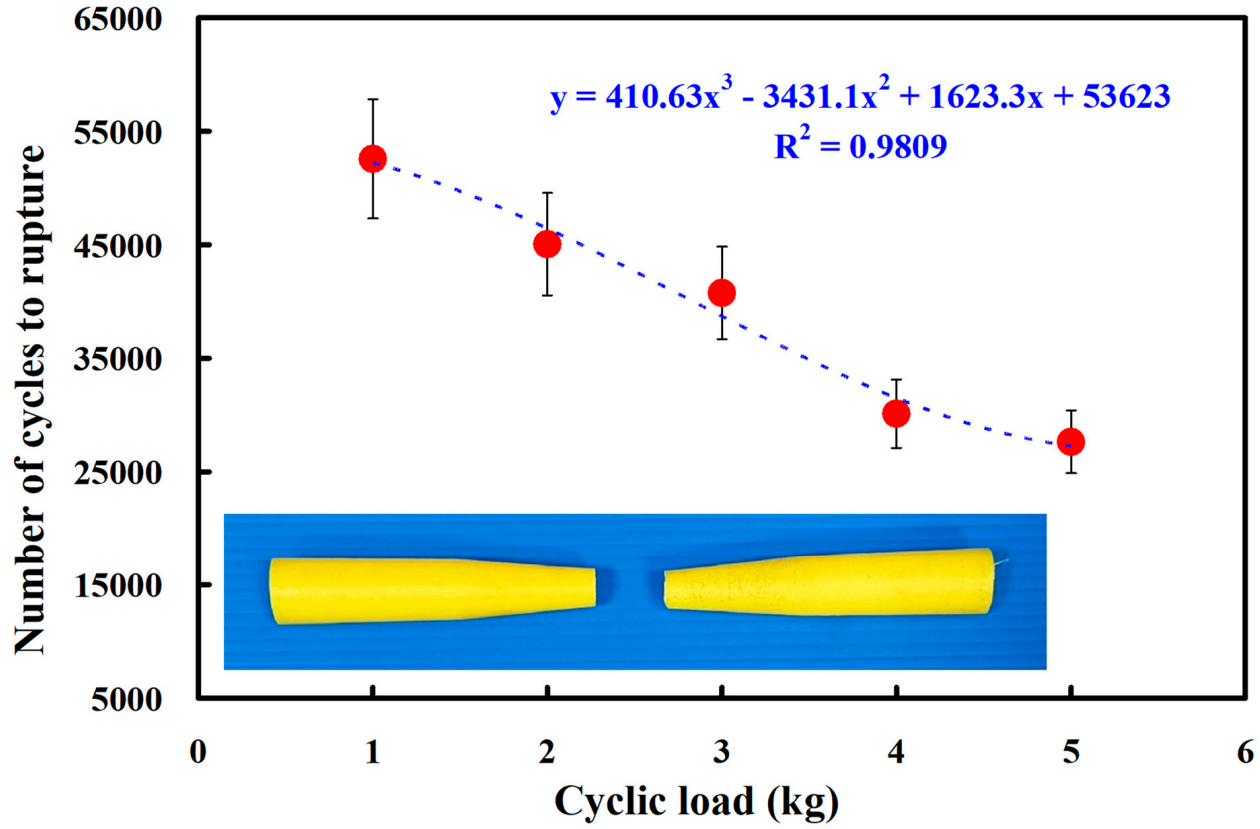

Figure 13. Fatigue test results of the RFW of ABS and ABS similar rods under five different cyclic loads.

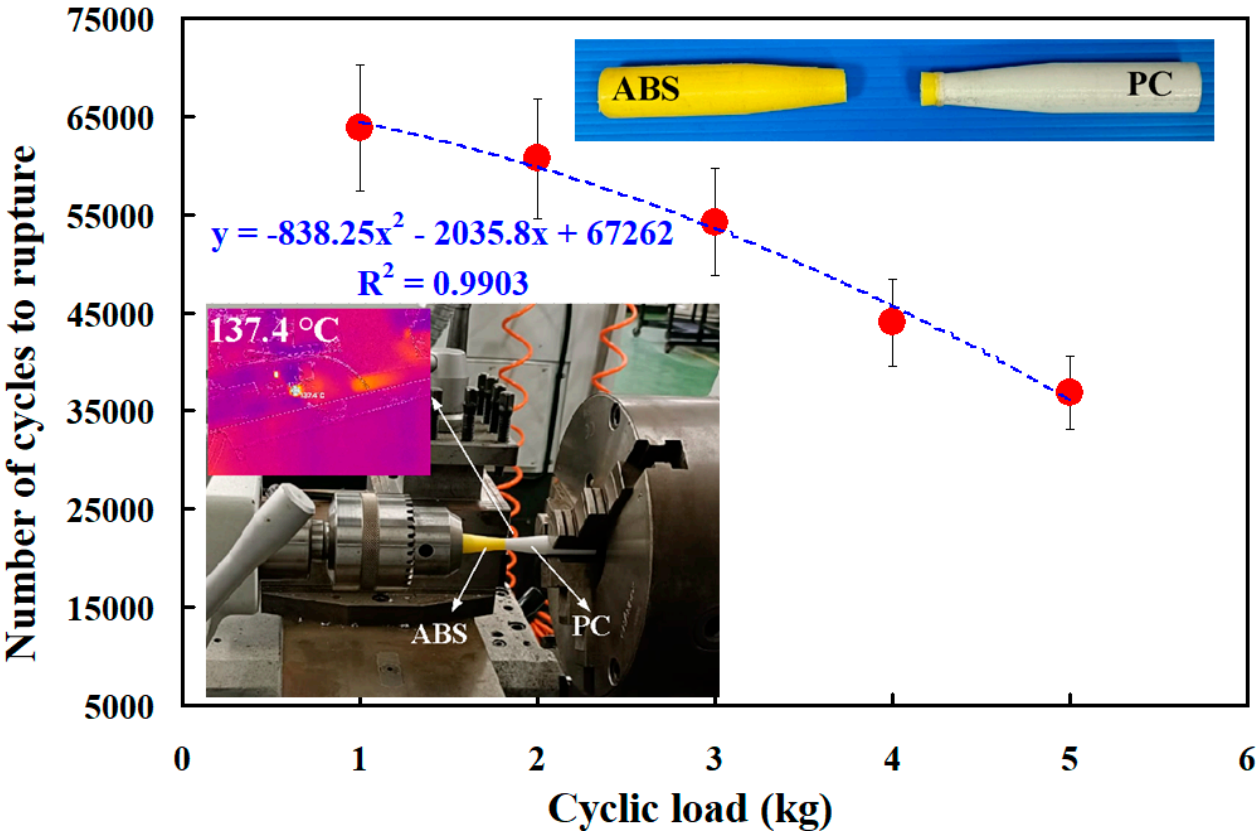

Figure 14. Fatigue test results of the RFW of ABS/PC dissimilar rods under five different cyclic loads.

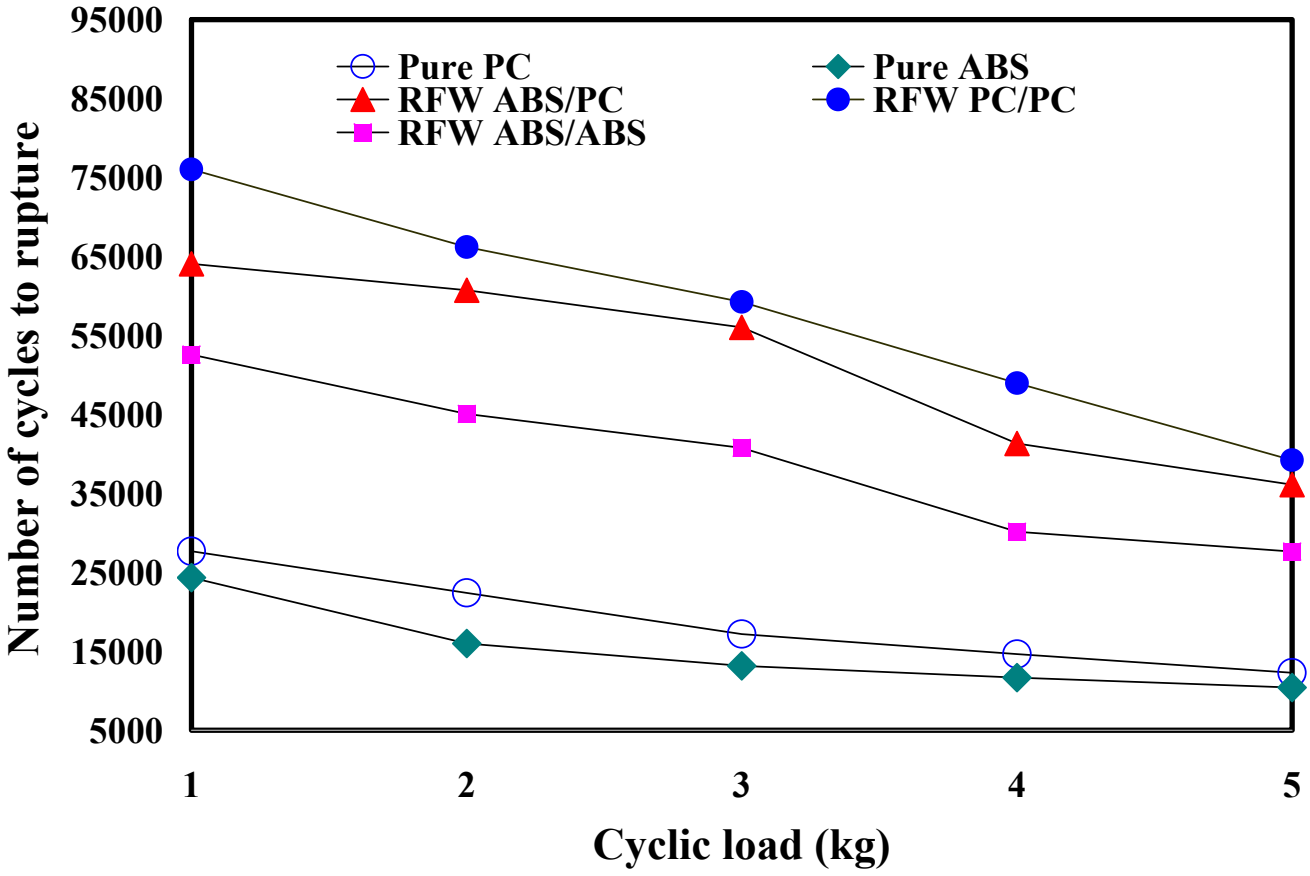

Figure 15. Fatigue test results of five different fatigue test specimens under five different cyclic loads.

Figure 16 shows the fatigue test results of the RFW of ABS and PC dissimilar rods under five different rotational speeds. The results showed that the average number of cycles until rupture of the RFW of ABS and PC using a rotational speed of 330 rpm, 490 rpm, 650 rpm, 950 rpm, and 1350 rpm was about 35,150, 39,120, 42,145, 48,957, and 53,240, respectively. It was found that the fatigue life of the RFW of ABS and PC increased with the increase in the rotational speed. This result shows that the weld strength in the weld interface was enhanced by increasing the rotational speed [37] due to the high peak temperature in the weld interface, resulting in high material flow during RFW. The average number of cycles until rupture (y) can be determined by the rotational speed (x) according to the prediction equation of $315.21x^2 + 2710.4x + 32{,}124$, with a correlation coefficient of 0.9907. It is interesting to note that the fatigue life of the RFW of ABS/PC is better than both the pure ABS and pure PC materials.

In general, RFW is a green manufacturing process that can reduce energy consumption compared with conventional arc welding. As a result, RFW meets the sustainable development goal 12 [38]. RFW is a practical method in various industries [39–41]. However, a lathe was used for the RFW in the current work. To reduce experimental error, the computer numerical control turning machine [42–45] was recommended to perform the RFW because the feed rate of RFW can be controlled precisely. In addition, the rotational speed [46] can be changed during the process of RFW. In addition, the rate of growth of a fatigue crack was not investigated using the Paris law [47–49]. Carbon dioxide laser [50–52] or fiber laser [52–55] have also been recommended as methods with which to join polymer rods. These topics are interesting research topics and are currently being investigated.

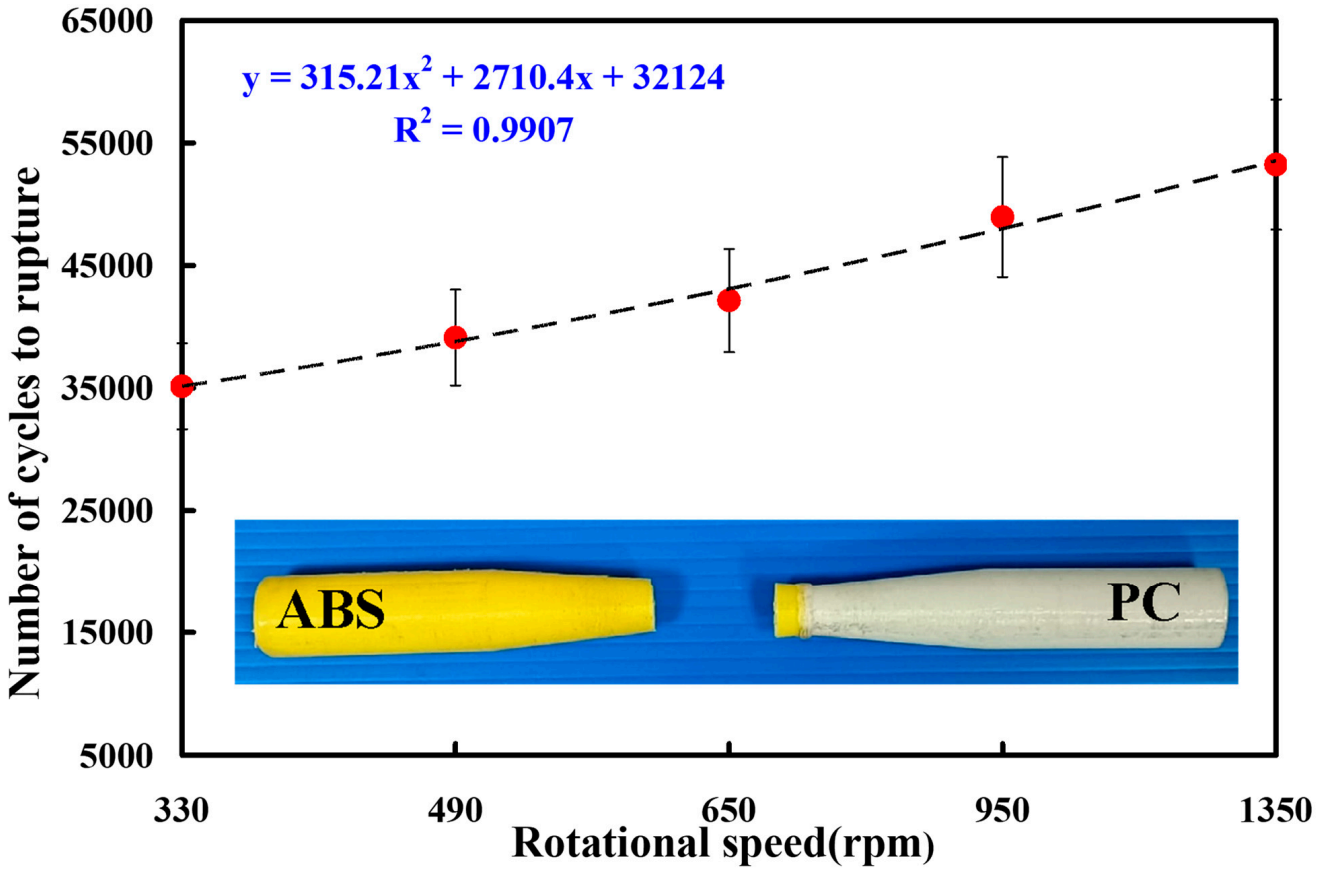

Figure 16. Fatigue test results of the RFW of ABS and PC dissimilar rods under five different rotational speeds.

4. Conclusions

The main aim of this study was to investigate the fatigue life of polymer parts fabricated using RFW. Five different cyclic loads were used to study the effects of loads on the fatigue life. The main conclusions from the experimental work in this study are as follows:

1. The fatigue failure mechanism of polymers is the same as that of metals.
2. The fatigue life of the RFW of PC/PC dissimilar rods is the best due to weld and integrity microstructural changes resulting from the combination of PC and PC materials. This result shows that the welding quality of the RFW of PC/PC dissimilar rods is robust for application in various industries.
3. The fatigue life of the RFW of ABS/PC is shorter under higher loads. The number of cycles until failure (y) can be determined by the cyclic load (x) according to the prediction equation of $y = -838.25x^2 - 2035.8x + 67{,}262$, with a correlation coefficient of 0.9903.
4. The fatigue life of the RFW of ABS/PC dissimilar components increases with an increased rotational speed. The number of cycles until rupture (y) can be determined by the rotational speed (x) according to the prediction equation of $315.21x^2 + 2710.4x + 32{,}124$, with a correlation coefficient of 0.9907.

Author Contributions: C.-C.K.: Wrote the paper, conceived and designed the analysis, and performed the analysis. N.G. and S.-H.H.: Collected the data and contributed data or analysis tools. All authors have read and agreed to the published version of the manuscript.

Funding: This study received financial support by the Ministry of Science and Technology of Taiwan under contract nos. NSTC 111-2221-E-131-015-MY2, MOST 110-2221-E-131-023 and MOST 109-2637-E-131-004.

Institutional Review Board Statement: Not applicable.

Data Availability Statement: Data and materials are available.

Conflicts of Interest: The authors declare no conflict of interest.

References

1. Isaeva, A.; Priymak, E.; Atamashkin, A.; Kirilenko, A. Optimization of rotary friction welding parameters for dissimilar joints of exploration drill pipes. *Int. J. Adv. Manuf. Technol.* **2023**, *126*, 5325–5337. [CrossRef]
2. Hassan, A.J.; Boukharouba, T.; Miroud, D. Concept of forge application under effect of friction time for AISI 316 using friction welding process. *Int. J. Adv. Manuf. Technol.* **2021**, *112*, 2223–2231. [CrossRef]
3. Bouarroudj, E.; Abdi, S.; Miroud, D. Improved performance of a heterogeneous weld joint of copper-steel AISI 1045 obtained by rotary friction using a metal powder insert. *Int. J. Adv. Manuf. Technol.* **2023**, *124*, 1905–1924. [CrossRef]
4. Li, B.; Liu, Q.; Jia, S.; Ren, Y.; Yang, P. Effect of V Content and Heat Input on HAZ Softening of Deep-Sea Pipeline Steel. *Materials* **2022**, *15*, 794. [CrossRef]
5. Delijaicov, S.; Rodrigues, M.; Farias, A.; Neves, M.D.; Bortolussi, R.; Miyazaki, M.; Brandão, F. Microhardness and residual stress of dissimilar and thick aluminum plates AA7181-T7651 and AA7475-T7351 using bobbin, top, bottom, and double-sided FSW methods. *Int. J. Adv. Manuf. Technol.* **2020**, *108*, 277–287. [CrossRef]
6. Huang, J.; Zhu, Z.; Wang, H.; Li, K.; Shi, W.; Jiao, T. Effect of WC Content on Microstructure and Properties of CoCrFeNi HEA Composite Coating on 316L Surface via Laser Cladding. *Materials* **2023**, *16*, 2706. [CrossRef]
7. Barakat, A.A.; Darras, B.M.; Nazzal, M.A.; Ahmed, A.A. A Comprehensive Technical Review of the Friction Stir Welding of Metal-to-Polymer Hybrid Structures. *Polymers* **2023**, *15*, 220. [CrossRef]
8. Bhukya, S.N.; Wu, Z.; Elmustafa, A.; Al-Allaq, A.; Ojha, M.; Mohammed, Y. Cu donor material assisted friction stir welding of AA2024 and AA6061 dissimilar alloys: Effect on downward force, temperature profile, and mechanical properties. *Int. J. Adv. Manuf. Technol.* **2023**, *127*, 3839–3851. [CrossRef]
9. Zhang, Z.; Wu, Q.; Zhang, H.W. Prediction of fatigue life of welding tool in friction stir welding of AA6061-T6. *Int. J. Adv. Manuf. Technol.* **2016**, *86*, 3407–3415. [CrossRef]
10. Shi, B.; Wang, L.; Zhan, X.; Lyu, F.; Gao, Z.; Shi, H. Weld morphology, microstructure evolution, and mechanical properties of laser beam welding of wire arc additive manufactured Al-Cu substrate. *Int. J. Adv. Manuf. Technol.* **2023**, *127*, 1935–1949. [CrossRef]
11. Liu, F.; Chen, W.; Deng, C.; Guo, J.; Zhang, X.; Men, Y.; Dong, L. Research advances in fatigue behaviour of clinched joints. *Int. J. Adv. Manuf. Technol.* **2023**, *127*, 1–21. [CrossRef]
12. Rayan, O.; Brousseau, J.; Belzile, C.; El Ouafi, A. Maraging steel powder recycling effect on the tensile and fatigue behavior of parts produced through the laser powder bed fusion (L-PBF) process. *Int. J. Adv. Manuf. Technol.* **2023**, *127*, 1737–1754. [CrossRef]
13. Ahmed, M.; Javidani, M.; Maltais, A.; Chen, X.-G. Welding of AA6061-T6 Sheets Using High-Strength 4xxx Fillers: Effect of Mg on Mechanical and Fatigue Properties. *Materials* **2023**, *16*, 3832. [CrossRef] [PubMed]
14. Su, W.; Cao, Q.; Cui, G.; Chen, Z. Investigations on Fatigue Life of Tube Connections Based on International Codes of Pressure Vessel. *Materials* **2023**, *16*, 231. [CrossRef] [PubMed]
15. Visco, A.; Scolaro, C.; Quattrocchi, A.; Montanini, R. Mechanical Characterization of Nanocomposite Joints Based on Biomedical Grade Polyethylene under Cyclical Loads. *Polymers* **2020**, *12*, 2681. [CrossRef] [PubMed]
16. Yu, Q.-Q.; Chen, T.; Gu, X.-L.; Zhang, N.-X. Fatigue Behaviour of CFRP Strengthened Out-of-Plane Gusset Welded Joints with Double Cracks. *Polymers* **2015**, *7*, 1617–1637. [CrossRef]
17. Koller, R.E.; Stoecklin, I.; Valet, S.; Terrasi, G.P. CFRP-Strengthening and Long-Term Performance of Fatigue Critical Welds of a Steel Box Girder. *Polymers* **2014**, *6*, 443–463. [CrossRef]
18. Popescu, D.; Baciu, F.; Vlăsceanu, D.; Marinescu, R.; Lăptoiu, D. Investigations on the Fatigue Behavior of 3D-Printed and Thermoformed Polylactic Acid Wrist–Hand Orthoses. *Polymers* **2023**, *15*, 2737. [CrossRef] [PubMed]
19. Park, S.J.; Son, Y.; Ahn, I.H. Influence of warm isostatic press (WIP) process parameters on mechanical properties of additively manufactured acrylonitrile butadiene styrene (ABS) parts. *Int. J. Adv. Manuf. Technol.* **2022**, *122*, 3311–3322. [CrossRef]
20. Ho, H.T.; Nguyen, N.H.; Rollet, M.; Phan, T.N.T.; Gigmes, D. Phosphonate-Functionalized Polycarbonates Synthesis through Ring-Opening Polymerization and Alternative Approaches. *Polymers* **2023**, *15*, 955. [CrossRef]
21. Papchenko, K.; Ricci, E.; De Angelis, M.G. Modelling across Multiple Scales to Design Biopolymer Membranes for Sustainable Gas Separations: 1—Atomistic Approach. *Polymers* **2023**, *15*, 1805. [CrossRef] [PubMed]
22. Wen, C.; Odle, R.; Cheng, S. Molecular Weight Distribution of Branched Polymers: Comparison between Monte Carlo Simulation and Flory-Stockmayer Theory. *Polymers* **2023**, *15*, 1791. [CrossRef] [PubMed]
23. Veliseicik, T.; Zurauskiene, R.; Kligys, M.; Dauksevic, M. Influence of Short Carbon Fibers on the Properties of Autoclaved Fiber Cement in Standard Fire Environment. *Materials* **2023**, *16*, 2513. [CrossRef] [PubMed]
24. Kladovasilakis, N.; Tsongas, K.; Kostavelis, I.; Tzovaras, D.; Tzetzis, D. Effective mechanical properties of additive manufactured triply periodic minimal surfaces: Experimental and finite element study. *Int. J. Adv. Manuf. Technol.* **2022**, *121*, 7169–7189. [CrossRef]
25. Lin, C.B.; Huang, P.J.; Chen, G.C. Integrating a fused deposition modeling 3D printing design with computer numerical control milling machines. *Int. J. Adv. Manuf. Technol.* **2023**, *125*, 3869–3880. [CrossRef]

26. Rodrigues, P.V.; Ramoa, B.; Torres, A.R.; Castro, M.C.R.; Machado, A.V. Enhancing the Interface Behavior on Polycarbonate/Elastomeric Blends: Morphological, Structural, and Thermal Characterization. *Polymers* **2023**, *15*, 1773. [CrossRef]
27. Jreije, A.; Mutyala, S.K.; Urbonavičius, B.G.; Šablinskaitė, A.; Keršienė, N.; Puišo, J.; Rutkūnienė, Ž.; Adlienė, D. Modification of 3D Printable Polymer Filaments for Radiation Shielding Applications. *Polymers* **2023**, *15*, 1700. [CrossRef]
28. Hubmann, M.; Groten, J.; Pletz, M.; Grießer, T.; Plevová, K.; Nemitz, W.; Stadlober, B. Influence of Injection Molding Parameters on the Peel Strength between Plasma-Treated Fluoropolymer Films and Polycarbonate. *Polymers* **2023**, *15*, 1568. [CrossRef]
29. Bulanda, K.; Oleksy, M.; Oliwa, R. Polymer Composites Based on Polycarbonate/Acrylonitrile-Butadiene-Styrene Used in Rapid Prototyping Technology. *Polymers* **2023**, *15*, 1565. [CrossRef] [PubMed]
30. Qi, M.; Cao, L.; Zhao, Y.; Jia, F.; Song, S.; He, X.; Yan, X.; Huang, L.; Yin, Z. Quantitative Analysis of Mixed Minerals with Finite Phase Using Thermal Infrared Hyperspectral Technology. *Materials* **2023**, *16*, 2743. [CrossRef]
31. Mahajan, A.M.; Babu, N.K.; Talari, M.K.; Rehman, A.U.; Srirangam, P. Effect of Heat Treatment on the Microstructure and Mechanical Properties of Rotary Friction Welded AA7075 and AA5083 Dissimilar Joint. *Materials* **2023**, *16*, 2464. [CrossRef] [PubMed]
32. Kuo, C.-C.; Gurumurthy, N.; Chen, H.-W.; Hunag, S.-H. Mechanical Performance and Microstructural Evolution of Rotary Friction Welding of Acrylonitrile Butadiene Styrene and Polycarbonate Rods. *Materials* **2023**, *16*, 3295. [CrossRef] [PubMed]
33. Hentati, F.; Hadriche, I.; Masmoudi, N.; Bradai, C. Optimization of the injection molding process for the PC/ABS parts by integrating Taguchi approach and CAE simulation. *Int. J. Adv. Manuf. Technol.* **2019**, *104*, 4353–4363. [CrossRef]
34. Stoporev, A.; Kadyrov, R.; Adamova, T.; Statsenko, E.; Nguyen, T.H.; Yarakhmedov, M.; Semenov, A.; Manakov, A. Three-Dimensional-Printed Polymeric Cores for Methane Hydrate Enhanced Growth. *Polymers* **2023**, *15*, 2312. [CrossRef]
35. Amza, C.G.; Zapciu, A.; Baciu, F.; Radu, C. Effect of UV-C Radiation on 3D Printed ABS-PC Polymers. *Polymers* **2023**, *15*, 1966. [CrossRef]
36. Milan, N.; Parenti, P.; Annoni, M.; Sorgato, M.; Lucchetta, G. Innovative fabrication of diffractive surfaces on plastic parts via textures micromilled on NiP injection moulds. *Int. J. Adv. Manuf. Technol.* **2021**, *113*, 1347–1359. [CrossRef]
37. Kuo, C.-C.; Chen, H.-W.; Xu, J.-Y.; Lee, C.-H.; Hunag, S.-H. Effects of Rotational Speed on Joint Characteristics of Green Joining Technique of Dissimilar Polymeric Rods Fabricated by Additive Manufacturing Technology. *Polymers* **2022**, *14*, 4822. [CrossRef]
38. Foltuţ, D.; Vălean, E.; Dzitac, V.; Moravian, L. The influence of temperature on the mechanical properties of 3D printed and injection molded ABS. *Mater. Today Proc.* **2023**, *78*, 210–213. [CrossRef]
39. Li, K.; Zhou, T.; Liu, B. Internet-based intelligent and sustainable manufacturing: Developments and challenges. *Int. J. Adv. Manuf. Technol.* **2020**, *108*, 1767–1791. [CrossRef]
40. Belkahla, Y.; Mazouzi, A.; Lebouachera, S.E.I.; Hassan, A.J.; Fides, M.; Hvizdoš, P.; Cheniti, B.; Miroud, D. Rotary friction welded C45 to 16NiCr6 steel rods: Statistical optimization coupled to mechanical and microstructure approaches. *Int. J. Adv. Manuf. Technol.* **2021**, *116*, 2285–2298. [CrossRef]
41. Barrionuevo, G.O.; Mullo, J.L.; Ramos-Grez, J.A. Predicting the ultimate tensile strength of AISI 1045 steel and 2017-T4 aluminum alloy joints in a laser-assisted rotary friction welding process using machine learning: A comparison with response surface methodology. *Int. J. Adv. Manuf. Technol.* **2021**, *116*, 1247–1257. [CrossRef]
42. Esangbedo, M.O.; Abifarin, J.K. Cost and Quality Optimization Taguchi Design with Grey Relational Analysis of Halloysite Nanotube Hybrid Composite: CNC Machine Manufacturing. *Materials* **2022**, *15*, 8154. [CrossRef] [PubMed]
43. Buhmann, M.; Carelli, E.; Egger, C.; Frick, K. Point cloud based tool path generation for corrective machining in ultra-precision diamond turning. *Int. J. Adv. Manuf. Technol.* **2022**, *120*, 6891–6907. [CrossRef]
44. Akhtar, M.N.; Sathish, T.; Mohanavel, V.; Afzal, A.; Arul, K.; Ravichandran, M.; Rahim, I.A.; Alhady, S.S.N.; Bakar, E.A.; Saleh, B. Optimization of Process Parameters in CNC Turning of Aluminum 7075 Alloy Using L27 Array-Based Taguchi Method. *Materials* **2021**, *14*, 4470. [CrossRef] [PubMed]
45. Liu, P.; Quan, Y.; Wan, J.; Yu, L. Experimental Investigation on the Wear and Damage Behaviors of Machined Wheel-Rail Materials under Dry Sliding Conditions. *Materials* **2021**, *14*, 540. [CrossRef]
46. Pang, Z.; Yang, J.; Cai, Y. Effects of Rotational Speed on the Microstructure and Mechanical Properties of 2198-T8 Al-Li Alloy Processed by Friction Spot Welding. *Materials* **2023**, *16*, 1807. [CrossRef]
47. Lv, Z.; Hou, R.; Cui, H.; Zhang, M.; Yun, H. Numerical study on fatigue crack behavior of 2024 Al alloy in abrasive waterjet peening. *Int. J. Adv. Manuf. Technol.* **2023**, *127*, 2979–2988. [CrossRef]
48. Ren, Y.; Liu, B.; Zhang, Y.; Dong, Y.; Jin, D.; Zhao, S.; Gao, J. The investigation of fracture characteristics and process optimization of low-cycle fatigue cropping by using an AET-based multi-sensor system. *Int. J. Adv. Manuf. Technol.* **2023**, *125*, 1371–1382. [CrossRef]
49. Yang, N.; Fu, S.; Tao, J.; Wang, H.; Yang, B.; Xu, J.; Guo, W.; Li, Z.; Zhang, L. Research on the reasonable loading method of staged follow-up rolling in low-stress cropping. *Int. J. Adv. Manuf. Technol.* **2022**, *120*, 8133–8151. [CrossRef]
50. Moritz, J.; Seidel, A.; Kopper, M.; Bretschneider, J.; Gumpinger, J.; Finaske, T.; Riede, M.; Schneeweiß, M.; López, E.; Brückner, F.; et al. Hybrid manufacturing of titanium Ti-6Al-4V combining laser metal deposition and cryogenic milling. *Int. J. Adv. Manuf. Technol.* **2020**, *107*, 2995–3009. [CrossRef]
51. Mansour, H.; Soliman, E.A.; El-Bab, A.M.F.; Abdel-Mawgood, A.L. Development of epoxy resin-based microfluidic devices using CO_2 laser ablation for DNA amplification point-of-care (POC) applications. *Int. J. Adv. Manuf. Technol.* **2022**, *120*, 4355–4372. [CrossRef]

52. Li, Y.; Geng, S.; Gu, S.; Huang, D.; Wang, Y.; Mi, G.; Jiang, P. Effect of liquid column on process stability and weld formation under ultra-high power fiber laser-arc hybrid welding of thick plates. *Int. J. Adv. Manuf. Technol.* **2022**, *121*, 8243–8255. [CrossRef]
53. Liu, S.Q.; Han, S.W.; Hwang, T.W.; Abolhasani, D.; Moon, Y.H. Design and application of laser scanning strategy for machining deep surface grooves with a continuous-wave fiber laser. *Int. J. Adv. Manuf. Technol.* **2023**, *127*, 4133–4147. [CrossRef]
54. Rushworth, A.G.A.; Xie, K.G.; Fang, B.L.; Shen, Y.X.; Huang, Z.P.; Zhang, X.Y. Generating Profiled Diamond Grinding Wheels by 2000 W Fiber Laser: On the Understanding of Laser Ablation Law with High Power and Establishment of a Predictive Model. *Int. J. Adv. Manuf. Technol.* **2022**, *120*, 3045–3063. [CrossRef]
55. Luo, Y.; Zhu, X.; Zhang, W.; Chang, C.; Gao, S.; Lu, B.; Yan, X. Modeling of tow-to-spot diameter ratio for laser cutting of single-layer carbon fiber–reinforced plastics (CFRP). *Int. J. Adv. Manuf. Technol.* **2023**, *127*, 4439–4452. [CrossRef]